Tribology Letters, Vol. 22, No. 1, April 2006 (© 2006)
DOI: 10.1007/s11249-006-9066-z

A hydrostatic laser surface textured gas seal

Y. Feldman, Y. Kligerman* and I. Etsion

Dept. of Mechanical Engineering, Technion – Israel Institute of Technology, Technion City, Haifa, 32000, Israel

Received 25 November 2005; accepted 12 April 2006; published online 7 June 2006

A theoretical model is developed to study the effect of partial laser surface texturing (LST) on a hydrostatic gas seal. The partial LST provides a mechanism for hydrostatic pressure build up in the sealing dam similar to that of a radial step. The surface texturing parameters are numerically optimized to obtain maximum efficiency in terms of the ratio of load carrying capacity over gas leakage. The performance of the optimum partial LST seal compares favorably with that of a radial step seal.

KEY WORDS: mechanical seals, gas lubrication, surface texturing

Notations

b	LST length
c	nominal clearance
d_i	internal seal diameter
d_o	external seal diameter
d_p	textured diameter
E	efficiency parameter, $E = \Delta P_{av}/Q$
h	local film thickness
h_{max}	maximum film thickness
h_{eq}	equivalent film thickness
h_p	dimple maximum depth
h_{pl}	dimple local depth
H	dimensionless film thickness, $H = h/c$
l	dimples column length
p	local pressure
p_a	ambient pressure
p_o	sealed pressure
P	dimensionless pressure, $P = p/p_a$
q_x^*	leakage in x direction
q_x	leakage per unit length
Q	dimensionless leakage, $Q = q_x \Big/ \left(\frac{c^3 \rho_a p_a}{12\mu l}\right)$
r	imaginary cell half length
R	imaginary cell dimensionless half length, $R = r/l$
S_p	area density
W	dimensionless load carrying capacity
x, z	Cartesian coordinates
x_l, z_l	local Cartesian coordinates
X, Z	dimensionless coordinates, $X = x / l$, $Z = z / l$
α	clearance ratio, $\alpha = h_{max}/c$
δ	dimensionless dimple diameter, $\delta = 2r_p/c$
ε	dimensionless dimple depth, $\varepsilon = h_p/c$
γ	texture portion or step location
μ	dynamic viscosity
ρ_a	density at ambient pressure

Indexes

av	average
LST	laser surface texturing
ps	parallel surfaces

*To whom correspondence should be addressed.
E-mail: mermdyk@techunix.technion.ac.il

1. Introduction

Surface texturing as a means for enhancing tribological properties of liquid lubricated mechanical components is well known for many years. Hamilton et al. [1] presented in 1966, a surface texturing in the form of micro asperities that act as micro hydrodynamic bearings in the case of parallel surfaces like in mechanical seals [2,3]. An etching technique was used to produce positive or negative asperity shapes. It was found that while load carrying capacity was almost the same with either shape of these asperities the lubricant leakage for the negative asperities was at least 10 times less than that for the positive ones.

Reactive ion etching (RIE) technique was investigated experimentally by Wang et al. [4] for load carrying capacity enhancement of SiC thrust bearings in water lubrication. Micro pits, produced by RIE, that were introduced on one of the bearing mating surfaces gave a two fold increase in critical load at transition from hydrodynamic to mixed lubrication compared to untextured surface. Wang and Kato [5] used RIE to improve the anti seizure ability of SiC seals working in water. Here again a two fold increase in critical load was obtained compared to untextured case.

So and Chen [6] investigated experimentally the main cause for considerable load carrying capacity appearance between two parallel sliding surfaces. The authors found that micro wedges formed by surface roughness asperities could generate a significant hydrodynamic effect. In a following paper [7] the authors proposed a theoretical model for analyzing this effect. The theoretical and experimental results were in good agreement when the sliding pairs operated in mixed lubrication conditions and the original surface roughness values were large. However, for very smooth surfaces the calculated friction force greatly overestimated the experimental results.

Etsion and Burshtein [8] presented a model for mechanical seals with regular micro surface structure, showing a substantial improvement in seal performance when evenly distributed hemispherical micro dimples are present on one of the mating seal surfaces. The micro structure can be attained by laser surface texturing (LST), which involves creation of an array of micro dimples on the seal surface by a material ablation process with a pulsed laser beam. The earlier model of [8] was followed by more in-depth theoretical and experimental studies e.g. Etsion et al. [9] who showed that the aspect ratio rather than the actual shape of the micro dimples is the most important parameter of the model. A high stiffness of the fluid film below a clearance of 1 μm was reported in [9] and a very good agreement was found with experimental results. Further testing of actual seals in water [10] showed large reduction of up to 65% in friction torque and to some 20 °C in face temperature. Similar results of lower friction and face temperature with laser textured seal face are reported in [11], where textured SiC rings were tested against carbon rings in oil. Another test of LST mechanical seal in oil [12] indicates 40% reduction in friction torque and nearly 100% increase of the LST seal service life.

The hydrodynamic effect by which LST causes reduction in friction torque depends on a local cavitation in each dimple and is therefore gradually diminishing at higher sealed pressures that eliminate this cavitation as was reported in [10]. To overcome this problem a partial LST was developed that enhances hydrostatic effects in high pressure seals [13]. This partial LST consists of higher density dimples over a certain portion of the sealing dam width adjacent to the high pressure side, leaving the remaining portion untextured. The textured portion provides an equivalent larger gap that results in converging clearance in the direction of pressure drop and hence, hydrostatic pressure build up. Experimental results reported in [13] showed that the partial LST can substantially reduce friction torque of high pressure liquid seals and increase the seal operating pressure limit. Another study [14] on both full and partial LST seals demonstrated its effect on reducing breakaway torque and blister formation in carbon-graphite mechanical seal faces. The benefits of partial LST were successfully demonstrated in applications other than mechanical seals that include hydrodynamic bearings [15,16] and piston rings [17,18].

The hydrodynamic effect generated by LST in liquids is also applicable in gas lubricated high speed seals as shown in a model by Kligerman and Etsion [19]. The main difference is the optimum dimple depth over diameter ratio, which in gas application is much smaller than in liquid application. This hydrodynamic effect was demonstrated experimentally in a test [20] where a substantial reduction in friction torque and face temperature, as well as more stable operation, was obtained with an LST seal configuration compared to an unntextured reference case at 12,000 rpm.

The main goal of the present paper is to analyze the potential benefit of partial LST in a hydrostatic gas seal, similar to that in liquid seals shown in reference [13].

2. The model

A schematic description of a partial LST mechanical seal is presented in figures 1 and 2. The textured face portion adjacent to the high pressure boundary at d_o extends from d_p to d_o. In typical mechanical seals the ratio of inner to outer diameter, d_i/d_o, is close to unity (around 0.9) and hence, seal curvature may be neglected. This allows treating the LST face as a collection of radial dimples columns as shown in figure 2(a). Each column has a length l equal to the radial width of the sealing dam and a LST length b equal to $(d_p-d_o)/2$. For a typical case with $d_o/2$ of order 10 mm, and a column width of order 0.1 mm, the angle of the circular sector being approximated with the rectangle is 0.01 Rad. A spherical segment with a base radius, r_p, and depth h_p (see figures 1 and 2b), models each one of the micro dimples. The micro dimples are distributed uniformly with an area density S_p, representing the percentage of the seal face area between d_p and d_o (see figure 2a) that is occupied by the dimples. Each micro dimple is located in the center of an imaginary square cell of sides $2r\times 2r$ (see figure 2b) were:

$$r = \frac{r_p}{2}\sqrt{\frac{\pi}{S_p}} \tag{1}$$

According to the basic assumptions adopted in this work the seal faces are separated by a uniform gas film thickness, c, (see figure 1). The sealed gas is compressible and viscous (Newtonian) with a constant viscosity μ.

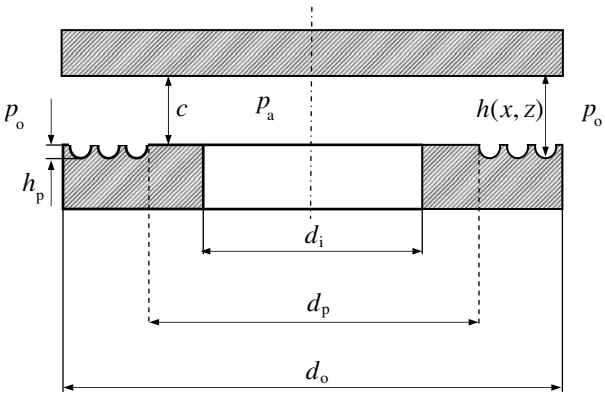

Figure 1. Schematic of a partial LST mechanical seal.

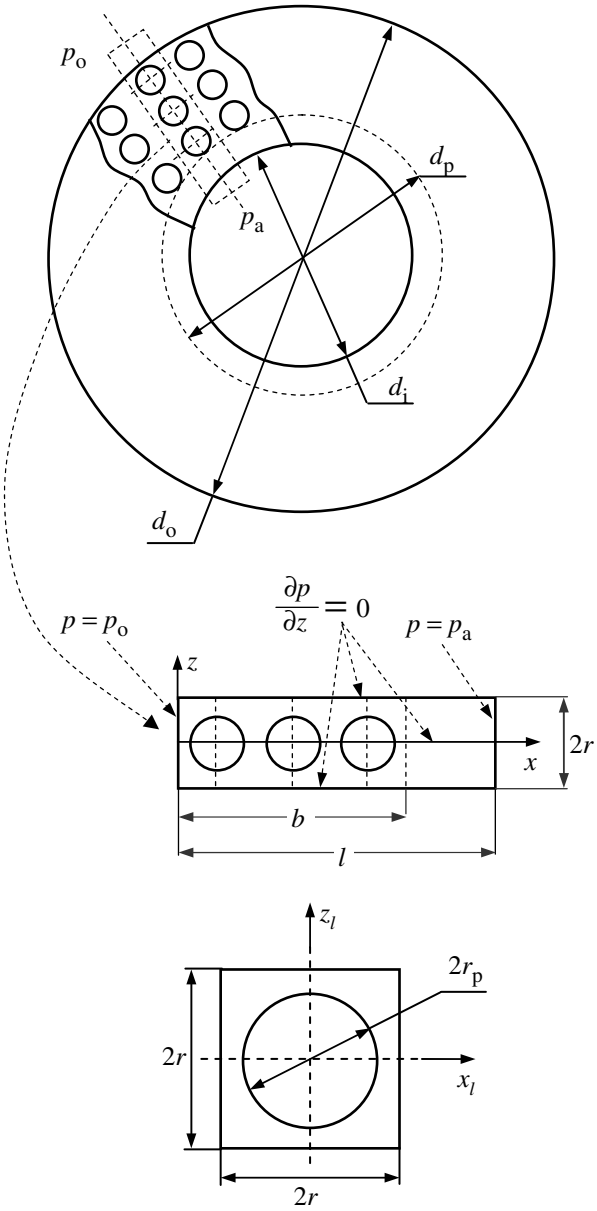

Figure 2. Geometry of a LST seal micro surface structure: (a) radial dimples column and boundary conditions; (b) individual cell with a single dimple.

The hydrostatic pressure distribution over a single dimples column for compressible Newtonian gas in laminar flow is obtained from the Reynolds equation:

$$\frac{\partial}{\partial x}\left(ph^3\frac{\partial p}{\partial x}\right)+\frac{\partial}{\partial z}\left(ph^3\frac{\partial p}{\partial z}\right)=0 \tag{2}$$

Note that the validity of this approach has been demonstrated in [21]. In equation (2) x and z are the Cartesian coordinates in the radial and circumferential directions, respectively as shown in figure 2(a). Periodicity of the surface texturing in the z direction, and symmetry (see figure 2a) about the x axis, permit solving the pressure distribution over just one half of one dimples column with the following boundary conditions:

$$p(x=0,z)=p_o; \quad p(x=l,z)=p_a \tag{3}$$

$$\frac{\partial p}{\partial z}(x,z=r)=\frac{\partial p}{\partial z}(x,z=0)=0 \tag{4}$$

The local film thickness, h, between the nominally parallel seal surfaces is given by:

$$h(x,z)=\begin{cases} c+h_{pl}(x_l,z_l) & \sqrt{x_l^2+z_l^2}\le r_p \\ c & \sqrt{x_l^2+z_l^2}>r_p \end{cases} \tag{5}$$

where the local dimple depth h_{pl} is:

$$h_{pl}(x_l,z_l)=\sqrt{\left(\frac{h_p^2+r_p^2}{2h_p}\right)^2-\left(x_l^2+z_l^2\right)}-\frac{r_p^2-h_p^2}{2h_p} \tag{6}$$

Two global coordinates x and z (see figure 2a) in equation (5) are related to the local coordinates x_l and z_l, within one control cell (see figure 2b), by $x=x_l+(2n-1)r$ and $z=z_l$, respectively, where n represents an ordinal number of the current imaginary control cell.

Equation (2) is rendered dimensionless by using a column length l to scale lengths, a nominal clearance c to scale the local film thickness and p_a to scale the pressure field, namely,

$$X=\frac{x}{l}; \quad Z=\frac{z}{l}; \quad H=\frac{h}{c}; \quad P=\frac{p}{p_a}; \tag{7}$$

The dimensionless global film thickness, $H(X,Z)$, is given by:

$$H(X,Z)=\begin{cases} 1+\sqrt{\left(\frac{\varepsilon}{2}+\frac{\delta^2}{8\varepsilon}\right)^2-\frac{l^2}{c^2}\left(X_l^2+Z_l^2\right)}-\left(\frac{\delta^2}{8\varepsilon}-\frac{\varepsilon}{2}\right), \\ \qquad\qquad X_l^2+Z_l^2<\frac{r_p^2}{l^2} \\ 1 \qquad X_l^2+Z_l^2\ge\frac{r_p^2}{l^2}, \end{cases} \tag{8}$$

where $\varepsilon = h_p/c$ is the dimensionless dimple depth and $\delta=2r_p/c$ is the dimensionless dimple diameter. The dimensionless global coordinates X and Z are related to the dimensionless local coordinates X_l and Z_l by: $X=X_l+(2n-1)r/l$ and $Z=Z_l$.

Substitution of the dimensionless parameters into equation (2) yields the Reynolds equation in its dimensionless form:

$$\frac{\partial}{\partial X}\left(PH^3\frac{\partial P}{\partial X}\right)+\frac{\partial}{\partial Z}\left(PH^3\frac{\partial P}{\partial Z}\right)=0 \tag{9}$$

Equation (9) is nonlinear, but by introducing a new dimensionless variable S defined as:

$$S=P^2 \tag{10}$$

it may be rewritten as a linear partial differential equation in S:

$$\frac{\partial}{\partial X}\left(H^3\frac{\partial S}{\partial X}\right)+\frac{\partial}{\partial Z}\left(H^3\frac{\partial S}{\partial Z}\right)=0 \qquad (11)$$

Equation (11) can be solved for the S distribution over a range of the independent dimensionless parameters; dimple diameter δ, dimple depth ε, textured portion γ, defined as $\gamma = b/l$ (see figure 2a), and the relevant boundary conditions defined in equations (12) and (13) for S:

$$S(X=0,Z)=P_o^2, \quad S(X=1,Z)=1 \qquad (12)$$

$$\frac{\partial S}{\partial Z}(X,Z=R)=\frac{\partial S}{\partial Z}(X,Z=0)=0 \qquad (13)$$

where $R=r/l$.

A finite difference method using a non-uniform grid (see figure 3) was used to solve the Reynolds equation (11) with its boundary conditions (12) and (13). The discretization of equation (11) leads to a set of linear algebraic equations for the nodal values of $S(X, Z)$. This equations set was solved using a successive over-relaxation Gauss-Seidel iterative method. The solution of equation (11) provides, through the transformation of equation (10), a dimensionless pressure distribution that can be integrated over the column area (see figure 3) to obtain its hydrostatic opening force W:

$$W=2\int_0^1\left(\int_0^R P dZ\right)dX \qquad (14)$$

The force W divided by the dimensionless column width $2R$ is the dimensionless average pressure P_{av}.

Because of symmetry conditions the pressure gradients in the z direction are equal to zero at $z=2r$ and $z=0$ (see figure 2a). Thus the gas leakage through the dimples column boundaries occurs only at $x=l$ and is given by:

$$q_x^*\,|_{x=l}=-\frac{c^3\rho_a}{12\mu}\int_0^{2r}\frac{\partial p}{\partial x}\,|_{x=l}\,dz \qquad (15)$$

Substituting the dimensionless coordinates and pressure definition given in equation (7) into equation (15), the gas leakage through the dimples column boundaries per unit width is defined as:

$$q_x\,|_{x=l}=\frac{1}{2r}q_x^*\,|_{x=l}=-\frac{1}{2r}\frac{c^3\rho_a p_a}{12\mu}\int_0^{2R}\frac{\partial P}{\partial X}\,|_{X=1}\,dZ \qquad (16)$$

The partial LST provides a mechanism for hydrostatic pressure build up in the sealing dam similar to that of a radial step (see figure 4a). This is due to the "collective" effect of the dimples [15] that, when close enough to each other, result in an effective higher equivalent clearance. Thus, it is interesting to compare the performance of the two similar configurations based on a common clearance ratio. The smaller the distance between the adjacent dimples of the LST the greater is its similarity to the step geometry. In the limiting case when neighboring dimples are touching each other the area density, S_p, is equal to 0.785. However, to prevent discontinues derivatives of film thickness between neighboring dimples that may invalidate the Reynolds equation (see Ref. [21]), the area density S_p in the present study was restricted to below 0.65.

The "equivalent step" height corresponding to the partial LST configuration (see figure 4b) is obtained by dividing the volume of a dimple by the area of its imaginary square cell, hence:

$$h_{eq}=\frac{\pi h_p}{24r^2}\left(h_p^2+3r_p^2\right) \qquad (17)$$

Thus, the clearance ratio α for an equivalent step configuration (defined by the ratio of maximum film thickness h_{max} to the nominal clearance c (see figure 4a)) is:

$$\alpha=\frac{h_{eq}+c}{c}=\frac{S_p\varepsilon}{6}\left(4\frac{\varepsilon^2}{\delta^2}+3\right)+1 \qquad (18)$$

The pressure distribution for the equivalent hydrostatic radial step seal was obtained from the analytical solution of equation (9) in its one dimensional form

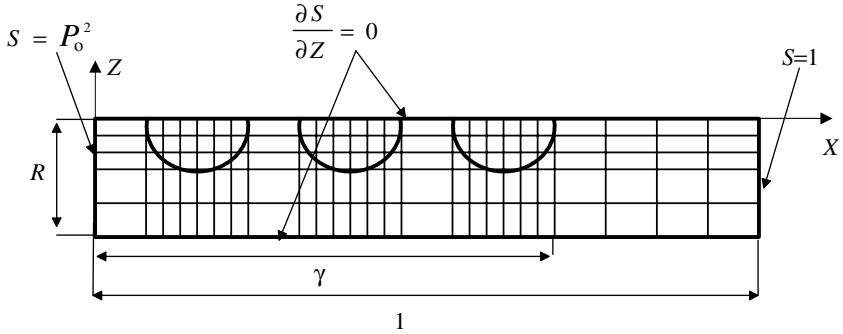

Figure 3. A dimensionless half dimples column model with boundary conditions for the variable S.

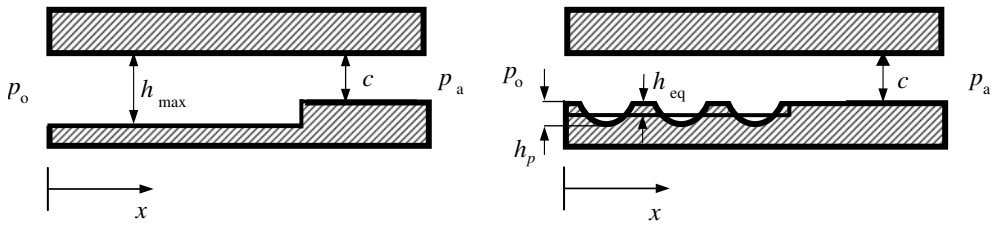

Figure 4. Schematic of an "equivalent step seal" (a), and its corresponding partial LST configuration (b).

(zero pressure gradients in the Z direction) with boundary conditions according to equations (12), hence:

$$P(X)=\begin{cases}\sqrt{\frac{\left(1-P_o^2\right)X}{\gamma-\alpha^3(\gamma-1)}+P_o^2}, & 0\le X<\gamma\\ \sqrt{\frac{\left(1-P_o^2\right)\alpha^3(X-1)}{\gamma-\alpha^3(\gamma-1)}+1}, & \gamma\le X\le 1\end{cases} \tag{19}$$

Substituting $\gamma=0$ and $\alpha=1$ into equation (19), yields the pressure distribution, P_{ps}, for a hydrostatic seal with completely smooth and parallel faces:

$$P_{ps}(X)=\sqrt{\left(1-P_o^2\right)X+P_o^2} \tag{20}$$

The performance of the radial step seal can be obtained by a somewhat cumbersome analytical integration of equation (19). However, by adopting the simpler integration approach used in [22] for a stepped piston in cylinders working with compressible fluid the results can be more readily obtained in the form:

$$P_{av}=\frac{2}{3}\gamma\frac{P_o^3-P_\gamma^3}{P_o^2-P_\gamma^2}+\frac{2}{3}(1-\gamma)\frac{P_\gamma^3-1}{P_\gamma^2-1} \tag{21}$$

where

$$P_\gamma^2=\frac{\gamma+\alpha^3P_o^2(1-\gamma)}{(1-\gamma)\alpha^3+\gamma}$$

Substituting $\gamma=0$ and $\alpha=1$ into equation (21) yields the relation for the average pressure, P_{avps}, for completely smooth and parallel surfaces in the form:

$$P_{avps}=\frac{2\left(P_o^2+P_o+1\right)}{3(P_o+1)} \tag{22}$$

The gas leakage per unit width for the step seal may be obtained by using equation (19) and it has the form:

$$q_x=-\frac{c^3\rho_a p_a}{12\mu l}\frac{\partial P}{\partial X}\Big|_{X=1}=-\frac{1}{2}\frac{c^3\rho_a p_a}{12\mu l}\frac{\left(1-P_o^2\right)\alpha^3}{\gamma-\alpha^3(\gamma-1)} \tag{23}$$

3. Results and discussion

3.1. Pressure distribution

Figure 5 presents pressure distributions along the center line of a dimples column for a hydrostatic partial LST seal (solid lines) and for its equivalent radial step seal (dashed lines, based on Eq. (21)). The results are shown for a typical case with 7 dimples $\gamma=0.7$, $S_p=0.65$, $\delta=100$, and $P_o=2$. The dimensionless dimple depth, ε, and its corresponding equivalent clearance ratio, α, are related according to equation (18). The pressure distribution for completely smooth and parallel surfaces, P_{ps} as given in equation (20) is also shown. Clearly, there is no optimum for either ε (LST seal) or α (radial step seal) in terms of higher pressure. Upon continuously increase of these two parameters a saturation of the pressure distributions is reached asymptotically.

The pressure distributions in figure 5 can be related to the tendency to prevent contact between the seal mating faces. It is clear from figure 5 that this tendency for the LST seal at any dimple depth ε is smaller than for its equivalent radial step seal. This may be explained by the fact that, for a same clearance c, a higher clearance ratio in the step configuration is associated with increasing of h_{max} while in the LST configuration it relates to increasing of h_p only (see figure 4). Hence, the LST seal presents higher resistance to inlet gas flow compared to the step seal while both configurations have similar resistance to the outlet gas flow. Obviously, a higher pressure buildup in the inlet region is required to maintain mass flow continuity in the case of higher inlet flow, resulting in a higher risk of face contact for the partial LST compared to the radial step configuration.

3.2. Load carrying capacity

The load carrying capacity relates to the difference ΔP_{av} between the average pressure, P_{av} for either the partial LST seal (see explanation following equation (14)) or the radial step seal (equation (21)), and the average pressure P_{avps} for completely smooth and parallel surfaces (see equation (22)).

Figure 6 shows the effect of the textured portion (or step location) γ on the average pressure difference, ΔP_{av} for three dimple depths, ε, values of partial LST seals (solid lines), and their corresponding cases of equivalent radial step seals (dashed lines). As can be seen for the three LST cases there is an optimum textured portion at about $\gamma=0.7$ for maximum load capacity. The three maximum ΔP_{av} values are in the range of $0.14<\Delta P_{av}<0.23$. This represents about 50% to 60% of the corresponding ΔP_{av} values for the equivalent radial step

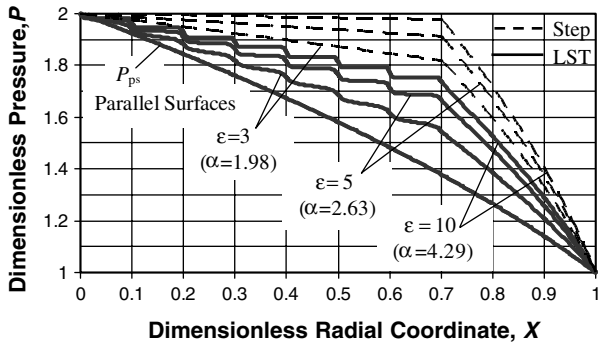

Figure 5. A comparison of pressure distributions along the center line of a dimples column and its equivalent step configuration, ($\gamma = 0.7$, $S_p = 0.65$, $\delta = 100$, $P_o = 2$).

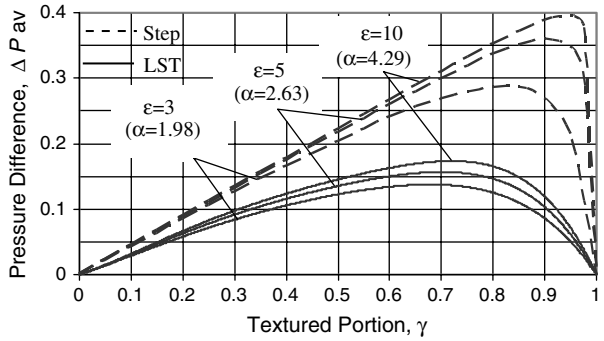

Figure 6. Average pressure difference, ΔP_{av}, versus textured portion (or step location), γ, ($\delta = 100$, $S_p = 0.65$, $P_o = 2$).

cases at the same $\gamma = 0.7$. Increasing the dimple depth from $\varepsilon = 5$ to $\varepsilon = 10$ leads to only about 12% increase in ΔP_{av} (see figure. 6). Further increase of the dimensionless dimple depth has marginal effect on the load capacity.

Contrary to the partial LST, the equivalent radial step seal is characterized by different optimum γ values for maximum ΔP_{av} depending on the α values (see figure 6). As the equivalent clearance ratio, α, increases a higher optimum γ (that approaches unity) is required to provide maximum load capacity. This may be explained by considering a constant maximum film thickness h_{max} for which, an increase in α means a decrease in the nominal film thickness c, leading eventually to complete blockage of the outlet flow (see figure 7). In this case the inlet pressure P_o prevails over the entire inlet region $0 \le X \le \gamma$ hence, resulting in higher load capacity as γ increases.

Figure 8 presents the effect of the dimensionless dimple diameter, δ, on the average pressure difference, ΔP_{av}, for three values of dimensionless dimple depth, ε. Note that since in our model the dimple shape is spherical its depth cannot exceed its diameter. This dictates a lower limit for the diameter over depth ratio in the form: $\delta/\varepsilon = 2r_p/h_p \ge 2$. Hence, for all the cases shown in figure 8, with $\varepsilon \le 15$, the dimensionless dimple diameter range to be considered is $\delta \ge 30$. As can be seen for the entire range of ε, the average pressure difference ΔP_{av} is independent of the dimensionless dimple diameter when $\delta > 60$. This is in agreement with the diminishing effect of $(\varepsilon/\delta)^2$ on the equivalent clearance ratio (see equation (18)) as δ increases for a given ε. Hence, while the load capacity of a partial LST seal depends on S_p, it is very insensitive to the dimple diameter $2r_p$ over the practical range of (ε/δ) values.

Figure 9 presents the percentage gains in average pressure difference, $\Delta\overline{P}_{av}$, having the from:

$$\Delta\overline{P}_{av} = 100\frac{P_{av} - P_{avps}}{P_{avps}} \tag{24}$$

as function of the sealed pressure, P_o, for three values of the dimensionless dimple depth, ε. As can be seen $\Delta\overline{P}_{av}$ increases slightly with increasing P_o and approaches asymptotically a limiting value that depends on ε. A same tendency was obtained for $\Delta\overline{P}_{av}$ of the equivalent radial step seal where the limiting value can be obtained from equations (21) and (22) for inlet pressure P_o approaching infinity:

$$\lim_{P_o\to\infty}\Delta\overline{P}_{av} = (1-\gamma)(1-\alpha^3)\left(\sqrt{\frac{\alpha^3(1-\gamma)}{\alpha^3(1-\gamma)+\gamma}} - 1\right)\times 100\% \tag{25}$$

It follows from equation (25) that a limit for $\Delta\overline{P}_{av}$ exists and it depends only on the geometrical parameters of the radial step seal, similar to the partial LST seal case.

3.3. Gas leakage

While high load capacity protects the seal mating faces from undesired contact that may cause high friction and wear, the main function of a good seal is to

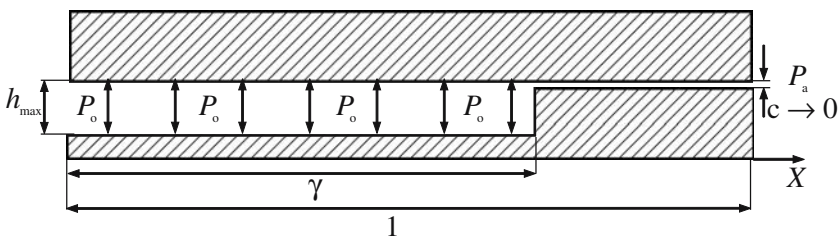

Figure 7. Pressure distribution for a step geometry with a complete blockage of the outlet flow.

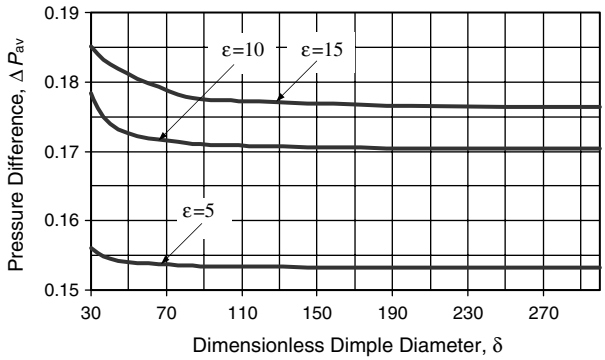

Figure 8. Average pressure difference, ΔP_{av} versus dimensionless dimple diameter, δ, at three dimple depth values, ($\gamma = 0.7$, $S_p = 0.65$, $P_o = 2$).

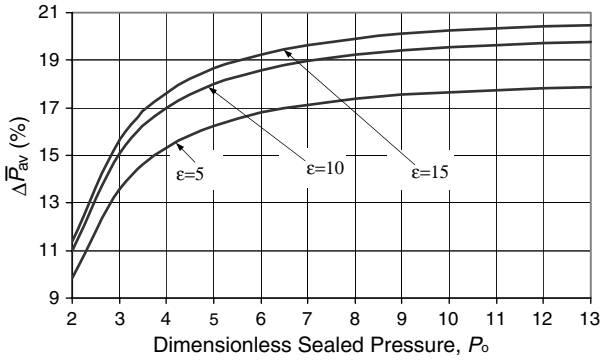

Figure 9. Average pressure gain $\Delta\overline{P}_{av}$ versus dimensionless sealed pressure P_o, ($\gamma = 0.7$, $\delta = 100$, $S_p = 0.65$).

prevent unacceptable leakage. Therefore, for a complete comparison of the partial LST and the equivalent radial step seals their gas leakage must also be considered. The dimensionless mass leakage per unit length (see equation (23) for example) is given in the form:

$$Q = q_x \Big|_{x=l} \Big/ \left(\frac{c^3 \rho_a p_a}{12 \mu l}\right) \tag{26}$$

Figure 10 presents the effect of the textured portion (or step location) γ on the dimensionless leakage for three dimple depths, ε, values of partial LST seals (solid lines), and their corresponding cases of equivalent radial step seals (dashed lines). At $\gamma = 0.7$, which is the optimum textured portion for maximum load capacity of partial LST seals (see figure 6), the leakage for the LST seal is about 30% less than that for the corresponding equivalent radial step seal. As can be seen from figure 10, the benefit of the LST seal in lowering the leakage compared to the step seal increases with increasing γ.

3.4. Efficiency Parameter, E

As was shown above the partial LST seal provides better sealing but at the same time has higher risk of friction and wear from face contact compared to its

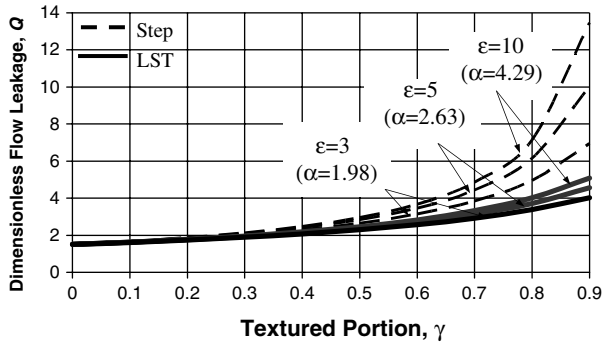

Figure 10. Comparison of the dimensionless gas leakage, Q, versus textured portion (or step location), γ, ($\delta = 100$, $S_p = 0.65$, $P_o = 2$).

equivalent radial step seal. Thus, in order to come up with an optimum design that minimizes the risks from face contact but also provides good sealing properties, an optimum seal design criterion (see also [22]) can be defined in the form:

$$E = \Delta P_{av}/Q \tag{27}$$

The best design would be the one that for a given average pressure difference, ΔP_{av}, will provide the smallest possible leakage, Q, and hence, will maximize E, which in the following will be referred to as the sealing efficiency parameter.

Figure 11 presents the efficiency parameter, E versus the textured portion, γ for two extreme cases of partial LST seals (solid lines) and their two corresponding

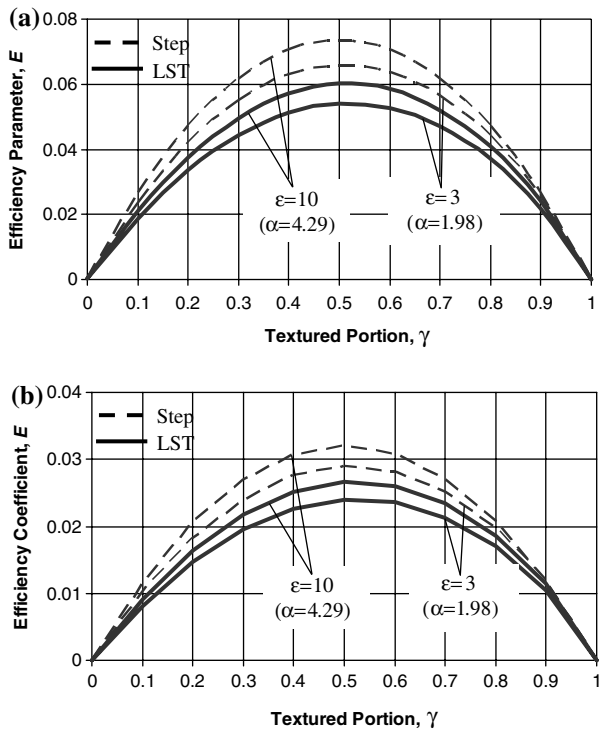

Figure 11. Comparison of the efficiency parameter, E, versus textured portion (or step location), γ: (a) $P_o = 2$; (b) $P_o = 5$, ($\delta = 100$, $S_p = 0.65$).

equivalent radial step seals (dashed lines). The results are presented for two dimensionless inlet pressures; $P_o = 2$ (figure 11a) and $P_o = 5$ (figure 11b). As can be seen from figure 11 the optimum seal design with maximum efficiency parameter (for both radial step and partial LST seals) corresponds to a textured portion or step location value of $\gamma = 0.5$. For $P_o = 2$, the maximum E values of the partial LST seal comprise about 80% of the corresponding maximum E values of the equivalent radial step seal. When the inlet pressure increases from $P_o = 2$ to $P_o = 5$ the two seal designs suffer about 50% reduction in their E values. Hence, the efficiency of the partial LST still remains 0.8 that of the equivalent step seal.

The effects of the dimple diameter, δ, and of the sealed pressure, P_o, on the efficiency parameter, E, were found to be very similar to their effects on the average pressure difference, ΔP_{av}, as presented in figures 8 and 9, respectively. Hence, both δ and P_o have little effect on E as they increase above a certain value. The most important finding is that the efficiency parameter of the LST seal is maintained about 0.8 of its corresponding value for the equivalent radial step seal over the full range of LST parameters and sealed pressures. This makes the partial LST concept an attractive design option for high pressure hydrostatic gas seals. The LST is much simpler and cost effective compared to other machining and texturing techniques [23], and, as was shown in the present analysis, is almost as efficient as the step design.

4. Conclusion

The potential of partial laser surface texturing for enhanced tribological performance of hydrostatic gas seals was numerically investigated. A detailed parametric analysis was performed to find the optimum laser texturing parameters for maximum seal efficiency. The LST dimples collective effect was found very similar to that of a Rayleigh step in terms of providing load capacity. The following conclusions summarize the results of the present study:

- The performance of a partial LST hydrostatic gas seal is mainly dependent on the dimples area density S_p, and is not affected by the dimple diameter $2r_p$. The highest load capacity is associated with high area density which practically can be as high as $S_p = 0.65$.
- The actual depth of the dimples has very little effect on the performance of a partial LST seal. Dimple depth that is from five to ten times the nominal seal clearance is sufficient.
- A textured portion value of $\gamma = 0.7$ provides maximum load capacity over a wide range of LST parameters and operating conditions.
- Lubricant leakage trough a partial LST seal is significantly less than that for a corresponding equivalent radial step seal.
- An efficiency parameter E can be defined and maximized for an optimum seal design that minimizes the risks from face contact but also provides good sealing properties
- A textured portion value (or step location) of $\gamma = 0.5$ is the optimum one for maximum efficiency parameter E of both partial LST and radial step seals. For this optimum case the maximum E values for the partial LST seal are about 80% of their corresponding ones for the equivalent radial step seal.

References

[1] D.B. Hamilton, J.A. Walowit and C.M. Allen, J. Basic Eng., Trans. ASME 88 (1966) 177.
[2] J.N. Anno, J.A. Walowit and C.M. Allen, J. Lubr. Technol., Trans ASME 90 (1968) 351.
[3] J.N. Anno, J.A. Walowit and C.M. Allen, J. Lubr. Technol., Trans ASME 91 (1969) 726.
[4] X. Wang, K. Kato, K. Adachi and K. Aizawa, Tribol. Int. 36 (2002) 189.
[5] X. Wang and K. Kato, Tribol. Lett. 14 (2002) 275.
[6] H. So and C. Chen, Tribol. Lett. 17 (2004) 513.
[7] H. So and C. Chen, Tribol. Lett. 19 (2005) 83.
[8] I. Etsion and L. Burstein, Tribol. Trans. 39 (1996) 677.
[9] I. Etsion, Y. Kligerman and G. Halperin, Tribol. Trans. 42 (1999) 511.
[10] I. Etsion, Proceedings of the 17th International Pump Users Symposium (2000) 17.
[11] X.Q. Yu, S. He and R.L. Cai, J. Mater. Process. Technol. 129 (2002) 463.
[12] A. Hoppermann and M. Kordt, O+P "Oelhydraulik und Pneumatik" 46 (2002) Vereinigte Fachverlage Mainz, ISSN 0341-2660.
[13] I. Etsion and G. Halperin, Tribol. Trans. 45 (2002) 430.
[14] S. Pride, K. Folkert, P. Guichelaar and I. Etsion, J. Lubr. Eng. 58 (2002) 16.
[15] V. Brizmer, Y. Kligerman and I. Etsion, Tribol. Trans. 46 (2003) 397.
[16] I. Etsion, G. Halperin, V. Brizmer and Y. Kligerman, Tribol. Lett. 17 (2004) 295.
[17] Y. Kligerman, I. Etsion and A. Shinkarenko, J. Tribol., Trans. ASME 127 (2005) 632.
[18] G. Ryk, Y. Kligerman, I. Etsion and A. Shinkarenko, Tribol. Trans. 48 (2005) 583.
[19] Y. Kligerman and I. Etsion, Tribol. Trans. 44 (2001) 472.
[20] A. McNikel and I. Etsion, J. Tribol., Trans. ASME 126 (2004) 788.
[21] Y. Feldman, Y. Kligerman, I. Etsion and S. Haber, J. Tribol., Trans. ASME 128 (2006) 345.
[22] I. Etsion, J. Fluids Eng., Trans. ASME 98 (1976) 494.
[23] I. Etsion, J. Tribol., Trans. ASME 127 (2005) 248.